THE 22nd CHESAPEAKE SAILING YACHT SYMPOSIUM
ANNAPOLIS, MARYLAND, MARCH 2016

Wind tunnel investigation of dynamic trimming on upwind sail aerodynamics

Aubin N., Naval academy research Institut - IRENAV, France [1]
Augier B., Naval academy research Institut - IRENAV, France
Bot P., Naval academy research Institut - IRENAV, France
Hauville F., Naval academy research Institut - IRENAV, France
Sacher M., Naval academy research Institut - IRENAV, France
Flay R. G. J., Yacht Research Unit, Department of Mechanical Engineering, The University of Auckland, New Zealand

ABSTRACT

An experiment was performed in the Yacht Research Unit's Twisted Flow Wind Tunnel (University of Auckland) to test the effect of dynamic trimming on three IMOCA 60 inspired mainsail models in an upwind ($AWA = 60°$) unheeled configuration. This study presents dynamic fluid structure interaction results in well controlled conditions (wind, sheet length) with a dynamic trimming system. Trimming oscillations are done around an optimum value of CF_{obj} previously found with a steady trim. Different oscillation amplitudes and frequencies of trimming are investigated. Measurements are done with a 6 component force balance and a load sensor giving access to the unsteady mainsail sheet load. The driving CF_x and optimization target CF_{obj} coefficient first decrease at low reduced frequency f_r for quasi-steady state then increase, becoming higher than the steady state situation. The driving force CF_x and the optimization target coefficient CF_{obj} show an optimum for the three different design sail shapes located at $f_r = 0.255$. This optimum is linked to the power transmitted to the rig and sail system by the trimming device. The effect of the camber of the design shape is also investigated. The flat mainsail design benefits more than the other mainsail designs from the dynamic trimming compared to their respective steady situtation. This study presents dynamic results that cannot be accurately predicted with a steady approach. These results are therefore valuable for future FSI numerical tools validations in unsteady conditions.

[1] nicolas.aubin@ecole-navale.fr

NOTATION

FSI	Fluid-structure interaction
VSPARS	Visual Sail Position And Rig Shape
YRU	Yacht Research Unit
A	Dynamic trimming amplitude (mm)
AWS	Apparent wind speed ($\mathrm{m\,s^{-1}}$)
AWA	Apparent wind angle ($°$)
c	Reference chord (m)
CF_i	Force coefficient in the i axis direction (-)
CF_{obj}	Optimization target coefficient (-)
CF_{sheet}	Force coefficient in the mainsail sheet (-)
f	Input frequency (Hz)
f_r	Reduced frequency (-)
F_i	Force in i axis direction (N)
F_{sheet}	Force in the main sail sheet (N)
h	Mainsail luff length (m)
L_{car}	Car traveller line length (mm)
L_{sheet}	Mainsail sheet length (mm)
$MSmax$	Mainsail with maximum camber for the design shape
$MSstd$	Mainsail with standard camber for the design shape
$MSflat$	Mainsail with zero camber for the design shape
P	Mechanical power from the sheet (mW)
q	Dynamic pressure (Pa)
S	Sail mould area ($\mathrm{m^2}$)
T	Time period of oscillation (s)
U_{ref}	Reference wind velocity ($\mathrm{m\,s^{-1}}$)
ρ	Density of air ($\mathrm{kg\,m^{-3}}$)

INTRODUCTION

A challenging task in yacht design modeling and simulation is the analysis of dynamic effects in the Fluid Structure Interaction (FSI) of the yacht sails and rig. The dynamic behavior can be caused by the sea state or the wind, but can

also be caused by the action of the crew while trimming. Literature has pointed out the difficulty of considering the realistic sailing environment of a yacht (Charvet *et al.*, 1996, Marchaj, 1996, Garrett, 1996). Recent studies have underlined the importance of considering the dynamic behavior: forced pitching motion in the wind tunnel (Fossati and Muggiasca, 2012), 2D simplified pitching (Gerhardt *et al.*, 2011), interaction of yacht sails in unsteady conditions (Gerhardt, 2010), full scale experiments and simulations (Augier *et al.*, 2012, 2013, 2014), and downwind sails (Collie and Gerritsen, 2006, Deparday *et al.*, 2014). Downwind sail design is where the gain from a dynamic aero-elastic analysis seems to be potentially the greatest due to the large motion and the induced large load variation. The main findings of these different studies are the same, i.e. the aerodynamics can be predicted more accurately with an unsteady approach.

To account for this dynamic behavior, several Dynamic Velocity Prediction Programs (DVPPs) have been developed (Masuyama *et al.*, 1993, Masuyama and Fukasawa, 1997, Richardt *et al.*, 2005, Keuning *et al.*, 2005) which need models of dynamic aerodynamic and hydrodynamic forces. While the dynamic effects on hydrodynamic forces have been studied extensively, the unsteady aerodynamic behavior of sails has received much less attention. (Schoop and Bessert, 2001) first developed an unsteady aeroelastic model in potential flow dedicated to flexible membranes but neglected the inertia. In a quasi-static approach, a first step is to add the velocity induced by the yacht's motion to the steady apparent wind to build an instantaneous apparent wind (Richardt *et al.*, 2005, Keuning *et al.*, 2005) and to consider the aerodynamic forces corresponding to this instantaneous apparent wind using force models obtained in the steady state.

Recently, advanced computational resources have enhanced numerical simulations and have allowed coupling of fluid and structural solvers dedicated to yacht sails (Renzsh and Graf, 2010, Chapin and Heppel, 2010, Trimarchi *et al.*, 2013, Ranzenbach *et al.*, 2013). In past years, IRENav and the K-Epsilon company have developed numerical tools dedicated to the simulation of the dynamic behavior of yacht sails. The FSI potential model ARAVANTI has been validated by full scale measurements (Augier *et al.*, 2012) and enables numerical studies of a yacht pitching in a head swell (Augier *et al.*, 2013, 2014), showing a clear break with the quasi-static approach. The recent RANS FSI coupling ARA-FINE™/Marine (Durand *et al.*, 2014) is required to simulate cases with strong separation for downwind simulations, but it is very time and CPU consuming.

Even though some advanced models are now available for sail aerodynamics, there is a real need for detailed validation of numerical simulations in order to provide reliable design tools for the sailing industry. Controlled experiments are also a great opportunity to understand the physics of FSI of yacht sails. Unfortunately, realistic and reliable experimental data is scarce and the validation of models in real conditions is difficult (Augier *et al.*, 2012, Fossati *et al.*, 2015). In this context, wind tunnel testing and full-scale testing are required for comparison and validation (Flay, 1996, Renzsch and Graf, 2013, Le Pelley *et al.*, 2002). Wind tunnel testing has the advantage of being in a controlled environment where a balance can be used to measure the forces created by the sails on the boat frame (Viola and Flay, 2010, Fossati, 2010, Fossati and Muggiasca, 2009, 2010, Wright *et al.*, 2010). Pressure and flying shape measurements can also be performed in wind tunnels (Lasher and Richards, 2007, Graf and Müller, 2009, Viola and Flay, 2011, Viola *et al.*, 2013). In a recent study, (Gerhardt *et al.*, 2011) developed an analytical model to predict the unsteady aerodynamics of interacting yacht sails in 2D potential flow, and performed 2D wind tunnel oscillation tests with a motion range typical of a 82-foot (25m) racing yacht (1992 International America's Cup Class). Recently (Fossati and Muggiasca, 2012, 2009, 2010, 2011) studied the aerodynamics of model-scale rigid sails in a wind tunnel, and showed that pitching motion has a strong and non-trivial effect on aerodynamic forces.

A dedicated experiment has been developed in the Yacht Research Unit Twisted Flow Wind Tunnel, University of Auckland, to study the aerodynamics of dynamic trimming. The model was simplified to a simple model-sized IMOCA 60 mainsail and a mast with no shrouds. We measured the effect of dynamic trimming on the forces (F_x, F_y) with the balance and the load in the sheet (F_{sheet}) for a given incoming wind ($U_{ref} = 3.5\,\mathrm{m\,s^{-1}}$ at $1.5\,\mathrm{m}$ height at model-scale location in an empty wind tunnel configuration) for 3 different sail design shapes.

In the first part of the paper, we describe the experimental set up and we define the optimum trimming. In the second part, the results are presented for different trimming oscillation amplitudes and frequencies and for different sail design shapes. Finally the influence of these different parameters on the global performance of the rig is discussed.

EXPERIMENTAL SETUP

Experiments were performed thanks to the Sailing Fluids collaboration program in the Twisted Flow Wind Tunnel of the Yacht Research Unit of the University of Auckland described in (Flay, 1996).

An 1/13th scale IMOCA 60 foot design mainsail was designed and built by INCIDENCE SAILS, using SAILPACK software developed by BSG DEVELOPPEMENTS, for these experiments. A system of three stepper motors and a control card was used in order to modify the main sheet length L_{sheet} and main car position L_{car} (see Fig. 1). Therefore, the mainsail trimming was imposed remotely without any human contact in the wind tunnel. The uncertainty of imposed trimming was estimated to be $\pm 2\,\mathrm{mm}$ through repeated measurements. Fig. 2 shows the $2.2\,\mathrm{m}$ long mast with the scaled mainsail in the $7.2\,\mathrm{m}$ wide by $3.5\,\mathrm{m}$ tall open jet test section of the YRU wind tunnel. Sail geometry is defined in Fig. 1. The rig is composed of a single $14\,\mathrm{mm}$ circular section carbon mast without spread-

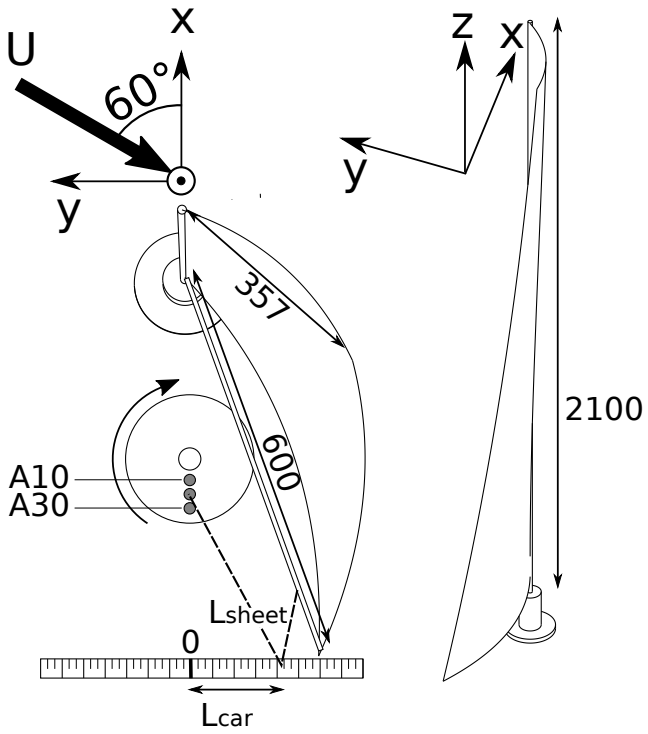

Figure 1: Experimental set up for dynamic trimming. Dimensions are in mm.

Figure 2: Model mainsail in YRU Twisted Flow Wind Tunnel, University of Auckland

ers, backstay or forestay. The objective is to create a simple bench experiment to study the aerodynamic effect of the dynamic trimming and to validate trimming optimization methods. The experiment includes Fluid Structure Interaction with mast deformation for use in numerical model comparisons. A six-component force balance located under the floor of the wind tunnel measures aerodynamic forces. The X-direction is aligned with the model longitudinal direction forward (driving force), the Y -direction is perpendicular positive port-side and measures the side force and the Z-direction is vertical as shown in Fig. 1. The balance precision was verified by calibration testing and the uncertainty on X, Y and Z axis are $\pm 0.09\,\mathrm{N}$, $\pm 0.11\,\mathrm{N}$ and $\pm 0.27\,\mathrm{N}$ respectively. A load sensor of $50\,\mathrm{N}$ range measures the sheet load with a precision of $\pm 0.02\,\mathrm{N}$. The flying shape is measured with five orange stripes (see Fig.2) through the VSPARS acquisition system (Le Pelley and Modral, 2008). The sampling frequency of the system measurement is $200\,\mathrm{Hz}$ and every run is recorded over $30\,\mathrm{s}$.

The velocity profile follows the empty wind tunnel boundary layer profile and is not twisted (no vanes in the flow). The apparent wind speed (AWS) is $U_{ref} = 3.5\,\mathrm{m\,s^{-1}} \pm 0.15\,\mathrm{m\,s^{-1}}$ - measured at $1.5\,\mathrm{m}$ high at the model-scale location in an empty configuration- and an apparent wind angle (AWA) set to $60° \pm 2°$.

A Pitot tube in the wind tunnel roof, was used to measure the dynamic pressure during each run. The mean value $\overline{q(t)}$ calculated for each test was used for the normalization of equations in order to correct for the possible fluctuations in the wind tunnel flow speed.

Optimum trimming

Different sail design shapes were tested. Three sails, made from the same sail cloth were designed with different cambers:

- MSstd = camber of the full scale sail (9.19% at the reference stripe)
- MSflat = no camber
- MSmax = more camber than MSstd (11.67% at the reference stripe)

A first test was performed in order to determine the best trim for the studied $AWA = 60°$. The model was placed on the balance and the sail was statically trimmed to the optimum $CF_{obj} = CF_x - 0.1|CF_y|$. This optimization target takes into account the contribution of the side force on the aerodynamic force and can be found in the design process of sailing yacht to consider the penalty due to the added hydrodynamic drag and leeway. For more details on the optimization function readers should refer to (Sacher *et al.*, 2015). Three stepper motors were used as winches to trim the sail: two motors used to trim the traveller position L_{car} and one centered motor used to trim the main sheet length L_{sheet}. Here we were looking for the best 2 trimming parameters (L_{sheet}, L_{car}). Optimum trimming was extracted from the test using the algorithm described in (Sacher *et al.*,

2016) and used as the reference for the dynamic trimming described in the following sections.

Dynamic trimming

The dynamic trimming consists of an oscillation in the sheet length L_{sheet} around the optimum trimming length obtained previously. The dynamic trimming was done with a fixed traveller position L_{car} (obtained from the optimum trimming) and the instantaneous sheet length $L_{sheet}(t)$ could be calculated from the controlled and recorded angular position of the rotating plate (see Fig. 3 and 1). $L_{sheet}(t)$, the instantaneous length of the sheet, is a function of A the amplitude of variation in mm, f the frequency of oscillation (rotation frequency of the stepper motor controlling the rotating plate) in Hz and the model-scale configuration geometry. The frequency f and amplitude A of oscillation were controlled by the rotating plate placed at the center-line of the boat as illustrated in Fig. 3. The sheet was connected to a pin fixed on the plate. The amplitude of oscillation depends on radial position of the pin. $A = 10\,\mathrm{mm}$ stands for an eccentric of $10\,\mathrm{mm}$ and corresponds to a peak to peak amplitude of motion of $20\,\mathrm{mm}$ on L_{sheet} (oscillation of L_{sheet} of $\pm 10\,\mathrm{mm}$).

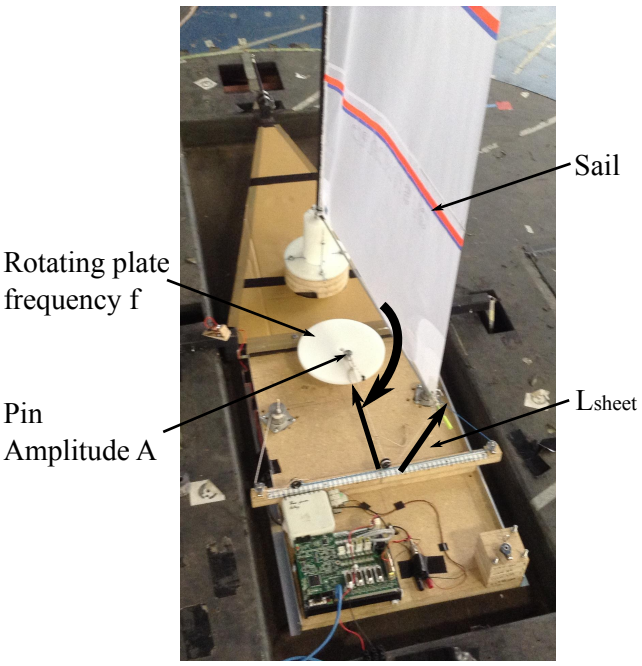

Figure 3: Experimental set up for dynamic trimming: rotating disk (photograph taken without wind)

RESULTS

We examine here the influence of the dynamic trimming on the aerodynamic forces of the sail. Three different sails were tested for 3 amplitudes of oscillation of $10\,\mathrm{mm}$, $20\,\mathrm{mm}$ and $30\,\mathrm{mm}$ and 7 ordered frequencies from $0\,\mathrm{Hz}$ to $3\,\mathrm{Hz}$. From these frequencies, non-dimensional reduced frequencies f_r are defined in the post processing parameters.

Post processing parameters

In this study we define the reduced frequency $f_r = f.c/U_{ref}$, with f the frequency of oscillation in Hz, c the reference chord length $c = S/h = 0.475\,\mathrm{m}$ and $U_{ref} = 3.5\,\mathrm{m\,s^{-1}}$ the reference flow speed. The reduced frequency is a non-dimensional indicator defined as the ratio of the oscillating motion to the reference convection time, from 0 to 0.38.

In the following part, aerodynamic forces and sheet loads are normalized as:

- the instantaneous aerodynamic driving force is defined using $CF_x(t) = \frac{F_x(t)}{\overline{q(t)}S}$
- its mean value presented in our study $CF_x = \overline{CF_x(t)} = \frac{\overline{F_x(t)}}{\overline{q(t)}S}$
- equivalent definition is used for the side force coefficient $CF_y = \overline{CF_y(t)} = \frac{\overline{F_y(t)}}{\overline{q(t)}S}$
- equivalent definition is used for the sheet load coefficient $CF_{sheet} = \overline{CF_{sheet}(t)} = \frac{\overline{F_{sheet}(t)}}{\overline{q(t)}S}$
- $q(t) = \frac{1}{2}\rho U(t)^2$ is the dynamic pressure measured during the run by the pitot tube.

Forces were averaged over an integer number of period of oscillation regardless of the reduced frequency in order to compare relevant mean values. Time series were filtered with a low pass filter frequencies defined as a Savitzky-Golay filter of order 1 of span 21 samples (Schafer, 2011).

Effect of the reduced frequency f_r

We focus here on the effect of the reduced frequency f_r on the forces for the case of the standard mainsail (MSstd) for an oscillation amplitude $A = 20\,\mathrm{mm}$ round the optimum L_{sheet}. Coefficients were averaged over the maximum number of integer oscillation periods found in the $30\,\mathrm{s}$ recording. Results are presented in Fig. 4. Measurements were doubled and showed good repeatability. Up and down triangles represent the maximum amplitude i.e. the maximum and minimum value of the time series.

For the first oscillation frequency studied, $f_r < 0.02$, the force coefficients decrease compared to the static situation $f_r = 0$ values. The oscillation is very slow and could be considered as quasi-steady. This quasi-steady oscillation around the optimum L_{sheet} degrades the performance because the sail is trimmed at a non-optimum point most of the time. For $f_r > 0.02$, dynamic trimming increases the mean force coefficient, which reaches a maximum around $f_r = 0.255$.

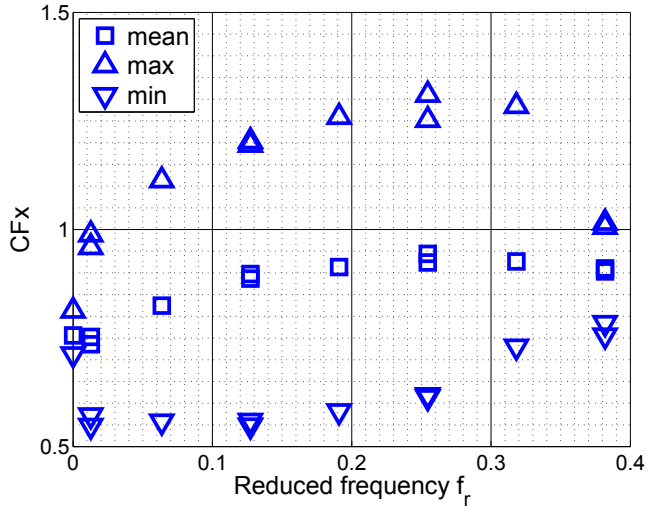

(a) CF_x for $A = 20\,\mathrm{mm}$

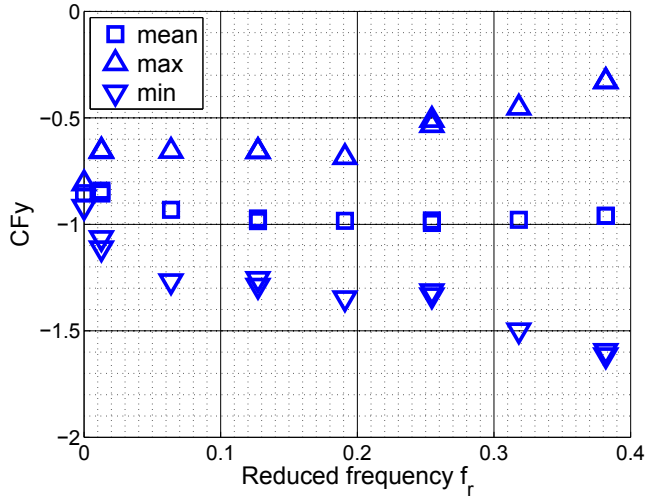

(b) CF_y for $A = 20\,\mathrm{mm}$

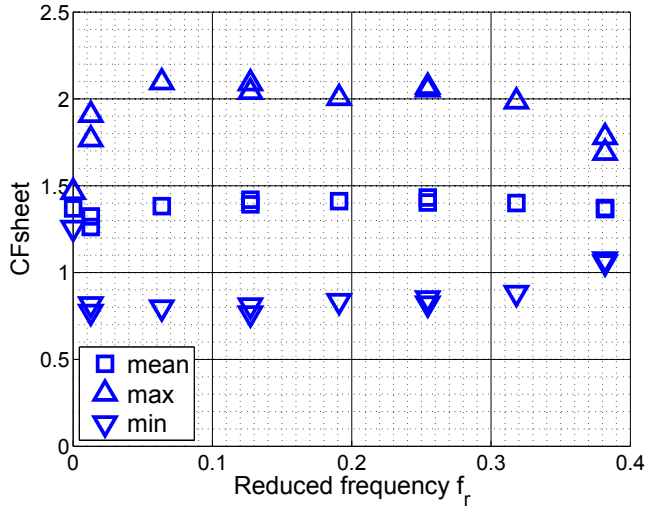

(c) CF_{sheet} for $A = 20\,\mathrm{mm}$

Figure 4: Effect of f_r at amplitude $A = 20\,\mathrm{mm}$ on CF_x (fig 4a), CF_y (fig 4b) and CF_{sheet} (fig 4c) for the standard mainsail. Up and down triangles represent the maximum and minimu amplitude of the time series respectively

The aerodynamic forces seem to benefit from an unsteady propulsion phenomenon due to the flapping of the sail. This unsteady propulsion is maximized for a defined range of frequencies and its effect decreases above $f_r = 0.255$. Amplitudes of variation of the force coefficients, illustrated by the triangles in Fig. 4, increase significantly until $f_r = 0.255$ and collapse dramatically at higher frequencies for CF_x and CF_{sheet}. In the case of CF_y, the amplitude of variation keeps increasing with the frequency of oscillation. The results show the effect of dynamic trimming compared to the steady trimming maximizes CF_x at a specific range of reduced frequency around 0.255.

Figs. 5 and 6 present the temporal evolution of the load in the sheet and the driving coefficient with the sheet length. This type of Lissajou representation was first proposed for a sailing yacht study by Fossati and Muggiasca (2009, 2010, 2011) in wind tunnel testing and was then used by (Augier *et al.*, 2013, 2014) in simulations and full scale measurements. For more clarity, signals are represented for only $12\,\mathrm{s}$. We present 4 of the 8 studied frequencies, but the trends are identical. The top graph illustrates the static case. The number of cycles represented increases with the frequency f_r. All the curves have been centered around their respective optimimum L_{sheet}, which are slightly different for the different design shapes. $L_{sheet} = 0\,\mathrm{mm}$ is set at the static optimum trim $L_{sheet\ static}$ for the optimum of the optimization target CF_{obj}.

CF_{sheet} vs L_{sheet} describes a loop which witnesses a hysteresis phenomenon (Fig. 5). In this case, the area inside the loop is the mechanical work exchanged with the rig system from the trimming stepper motor. The counter-clockwise sense of rotation, indicated by the arrow on the figure, shows that the work is negative, i.e. given to the system. This confirms that the sail and rig system are forced by the motion of the sheet for the whole range of studied frequencies. The area in the loop increases slightly until $fr = 0.255$ where it reaches a maximum. The loop collapses at $fr = 0.38$. The work exchanged with the rig system is a maximum at $fr = 0.255$ which corresponds to the optimum CF_x observed in Fig. 4a.

CF_x vs L_{sheet} describes a loop as well (Fig. 6). One should realise that the area inside the loops is not actual physical work however it follows the same trend as the work energy from F_x along the x-direction. It is very interesting to observe that the sense of rotation switches for the different frequencies. For $f_r = 0.013$ and 0.38, the system dissipates energy as it turns counter-clockwise. The system gains energy from the oscillation at $f_r = 0.255$ (clockwise rotation). The $f_r = 0.127$ case is a transition where the loop describes a figure 8 shape.

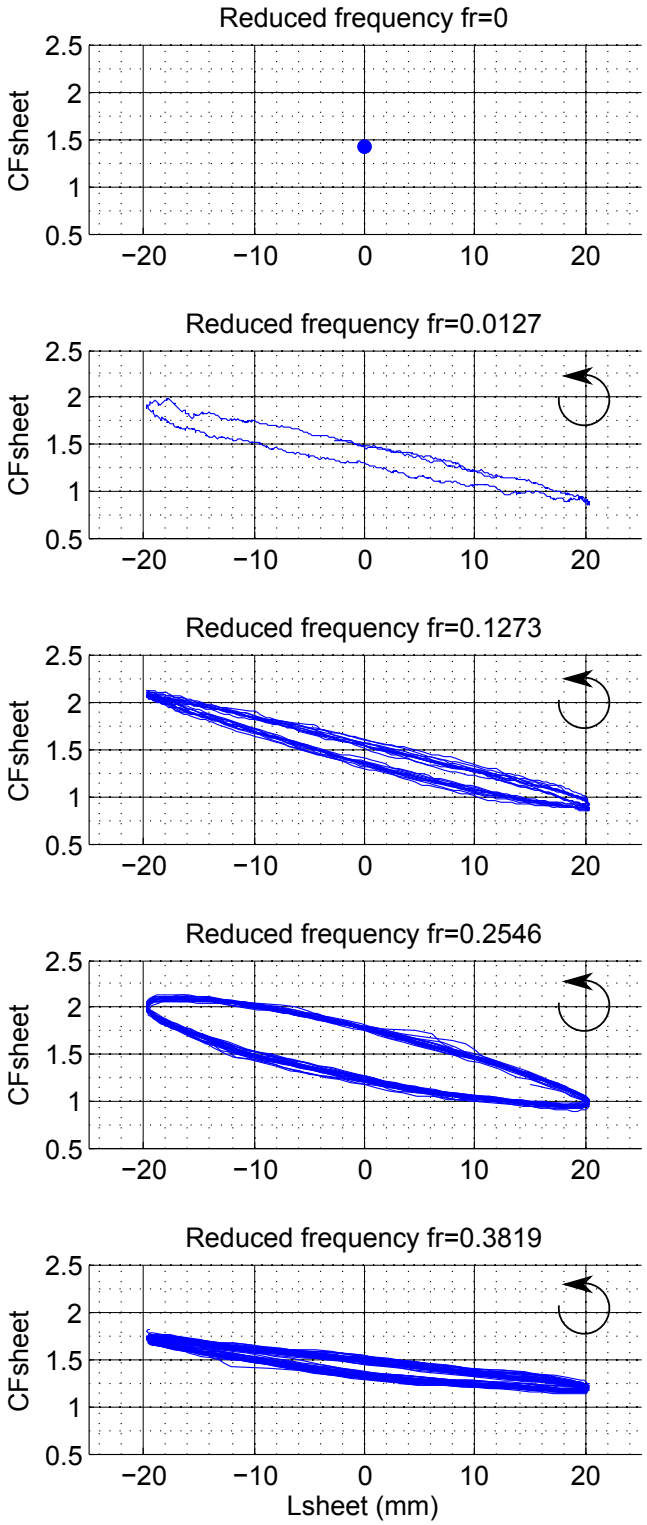

Figure 5: Evolution of CF_{sheet} with L_{sheet} at amplitude $A = 20\,\mathrm{mm}$ for the standard mainsail for different reduced frequencies. Signals are presented for $12\,\mathrm{s}$. The steady part was done without load sensor, so no steady load sheet is available for this configuration.

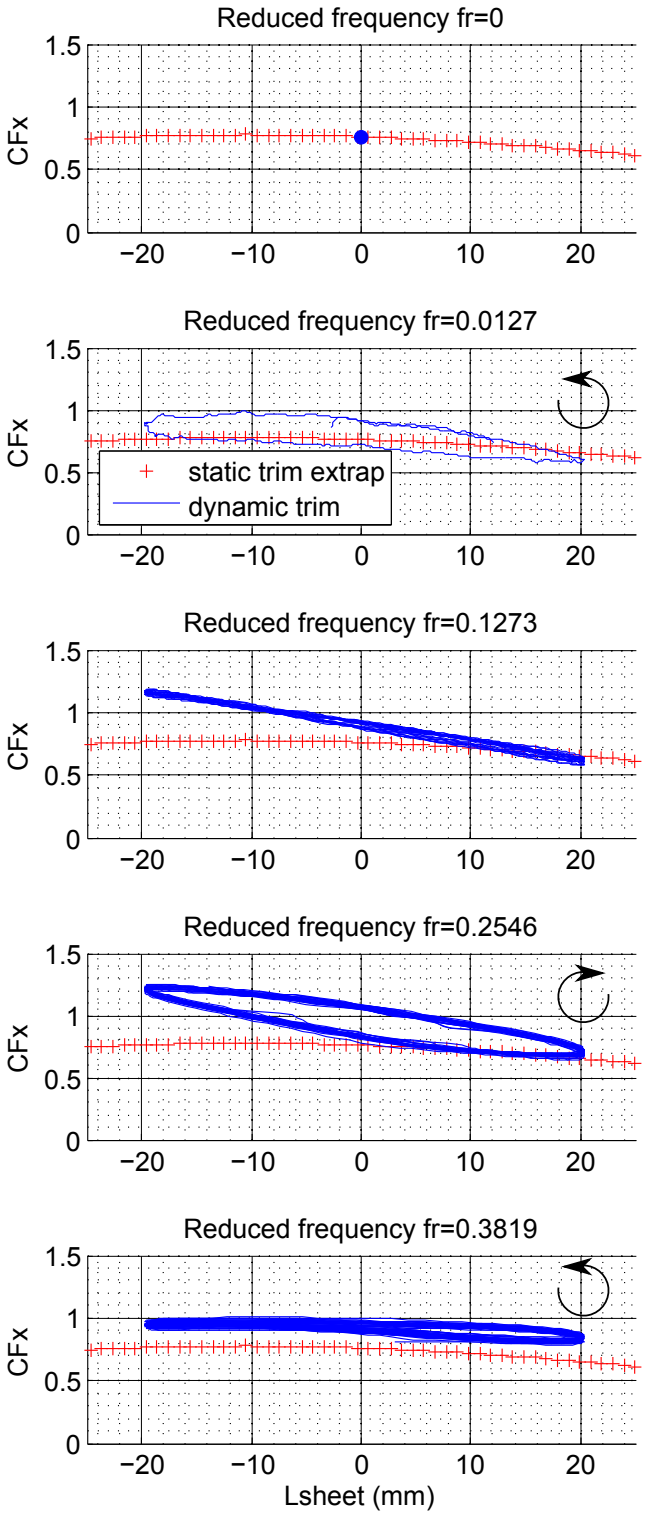

Figure 6: Evolution of CF_x with L_{sheet} at amplitude $A = 20\,\mathrm{mm}$ for the standard mainsail for different reduced frequencies. Signals are presented for $12\,\mathrm{s}$. Red crosses represent the steady state extrapolated from the 2D optimization part data.

Power is calculated at each reduced frequency and presented in Fig. 7. Power is proportional to the area in the loop illustrated in Fig. 5 and is defined as:

$$P = \frac{\overline{q(t)}S}{T} \oint_{one\ loop} CF_{sheet}(L_{sheet})dL_{sheet}$$

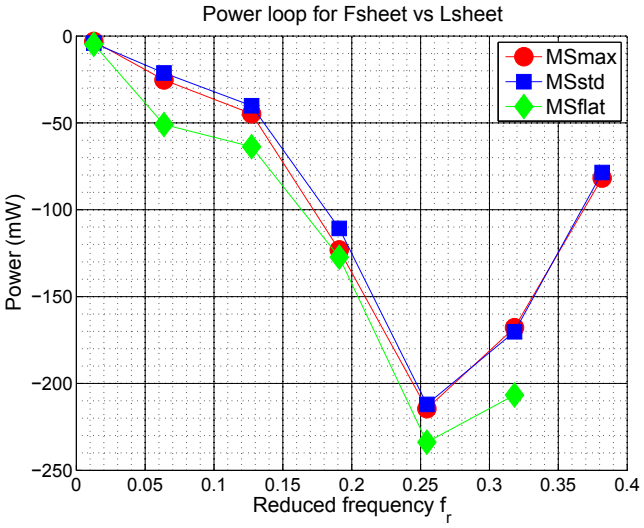

Figure 7: Power given to the system by the sheet oscillation forcing at $A = 20\,\mathrm{mm}$. Power is proportional to the area in the loop represented in Fig. 5

The power value shown on Fig. 7 is the averaged value of each power value calculated using the previous equation on each entire period oscillation loop. The exchange of energy of the forcing is related to the maximum of force obtained at $f_r = 0.255$ and the sudden collapse of the amplitude of variation of CF_x and CF_{sheet} at $f_r = 0.38$. Nevertheless a part of the trend observed in the force coefficient needs to be explained by studying the other parameters of the other forcing parameters such as the sail camber i.e. the design shape.

Effect of the design shape

The effects of the reduced frequency f_r on the forces are presented for the 3 design shapes and the 3 amplitudes of oscillation. For each sail, the trimming oscillation is done around its specific optimum. $L_{sheet\ Static}$ are different for each case. Again, coefficients are averaged over the maximum number of full oscillation periods found in the 30 s recording. Results are presented in Figs. 8, 9 and 10, CF_x, CF_{sheet} and CF_{obj} respectively. Oscillation amplitudes (maximum and minimum value) of force coefficients are not displayed for clarity but trends are identical to those described in the previous section. Due to the parameters of the optimum trimming (L_{sheet}, L_{car}) for the flat mainsail design shape, high frequency oscillations could not be explored at $A = 30\,\mathrm{mm}$ because the forcing was too strong. The general trends described in the previous section are identical for the 3 studied sail design shape and the different amplitudes of oscillation. The tendencies observed at $A = 20\,\mathrm{mm}$ are amplified at greater amplitude $A = 30\,\mathrm{mm}$ and slightly minimized at $A = 10\,\mathrm{mm}$.

It is interesting to notice that the effect of the dynamic trimming is greater for the flat mainsail design MSflat. The CF_x coefficient are nearly identical for the two cambered sails for $A = 10\,\mathrm{mm}$ and $A = 20\,\mathrm{mm}$ whereas the static performances are significantly worse. It seems that the dynamic behavior due to flapping catches/compensates for the defect of flat mainsail design MSflat in static conditions. The unsteady propulsion phenomenon is high enough to compensate for the poor aerodynamic performance of the flat sail in a steady trimming. The oscillation needs a minimum of amplitude of $A > 10\,\mathrm{mm}$ to have a significant effect on the MSflat. However, the optimum of MSflat is reached for a specific frequency $f_r = 0.255$ and decreases rapidly around this value, unlike the other sails MSmax and MSstd where the range of optimal frequencies is wider.

The load in the sheet in static situations i.e. $f_r = 0$ is linked to the camber (Fig. 9). The static CF_{sheet} is greater for the maximum camber mainsail MSmax and it is identical for the two other sails. Variations in the load in the sheet CF_{sheet} for different frequencies are consistent with the effect of dynamic trimming observed on MSflat. The trends are identical with CF_x. At low oscillation amplitudes, the sheet tension increases significantly for the flat sail until $f_r = 0.32$, when the CF_{sheet} reaches a maximum and decreases slightly after $f_r = 0.13$ for the other sails. For $A = 20\,\mathrm{mm}$, the maximum load in the sheet is reached at lower frequencies but a greater load is still necessary to make the flat sail oscillate. It seems that at these amplitudes, the energy brought to the system by the forced oscillation is greater in the case of MSflat, which explains the important gain on the aerodynamic coefficients observed in Figs. 5 and 6. The differences between the sails are smoothed at $A = 30\,\mathrm{mm}$ in CF_{sheet}, as illustrated by the energy brought to the system in CF_x and CF_y. Energy brought to the system by the oscillation of the sheet is illustrated in Fig. 7. The power exchanged is a maximum at $f_r = 0.255$.

The CF_{obj} evolution shown in Fig. 10 depends on both the camber of the sail and the amplitude of oscillation. For the low oscillation $A = 10\,\mathrm{mm}$ in Fig. 10a, the optimization target shows a maximum for the flat mainsail design contrary to the standard and maximum camber designs which present a plateau from $f_r = 0.255$. This plateau disappears for higher amplitude oscillations and all the curves present a maximum. The maximum camber design presents either the best optimization value or is fairly close to the maximum optimization target value regarding the different oscilation frequencies and amplitudes. For this $AWA = 60°$ this trend confirms the sailors' knowledge causing them to try to increase the camber by easing the outhaul of the sail to improve their performance in a situation such as a dogleg while sailing perpendicular to the true wind direction.

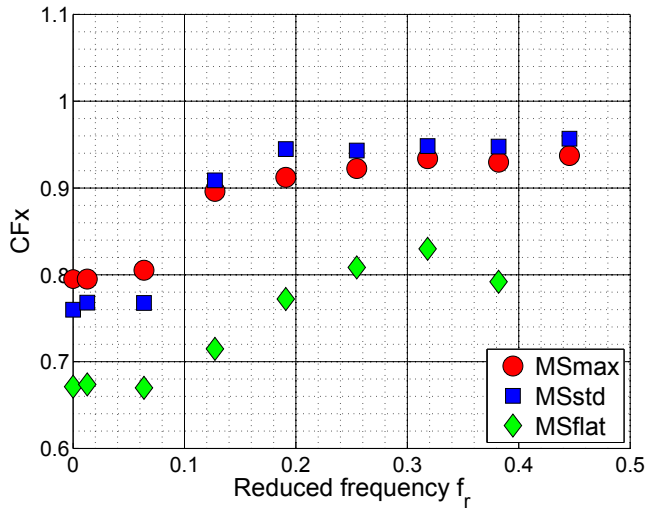

(a) $A = 10\,\mathrm{mm}$

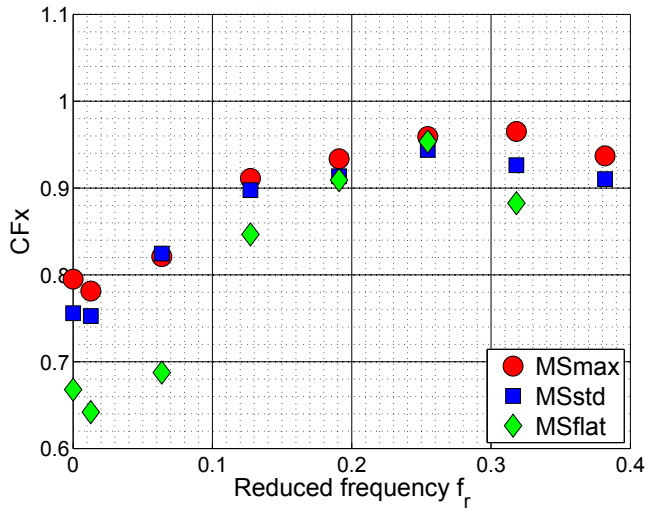

(b) $A = 20\,\mathrm{mm}$

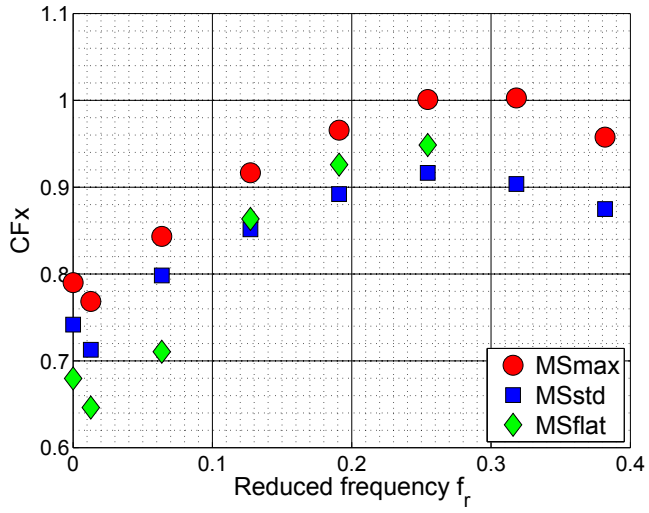

(c) $A = 30\,\mathrm{mm}$

Figure 8: Effect of f_r on CF_x for the 3 design shape at amplitude (a) $A = 10\,\mathrm{mm}$, (b) $A = 20\,\mathrm{mm}$ and (c) $A = 30\,\mathrm{mm}$.

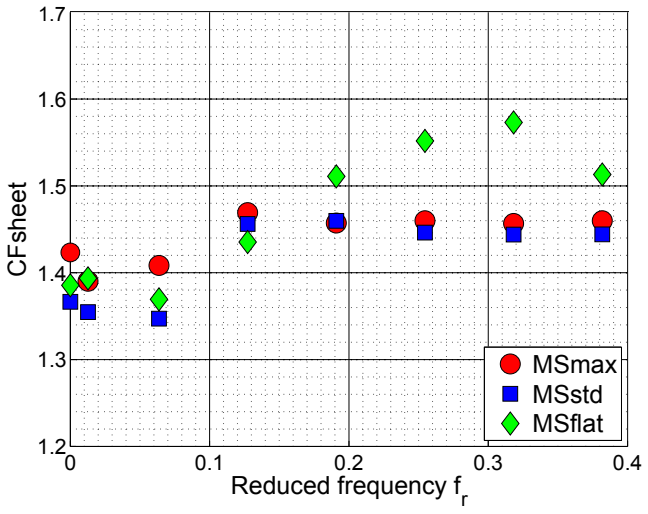

(a) $A = 10\,\mathrm{mm}$

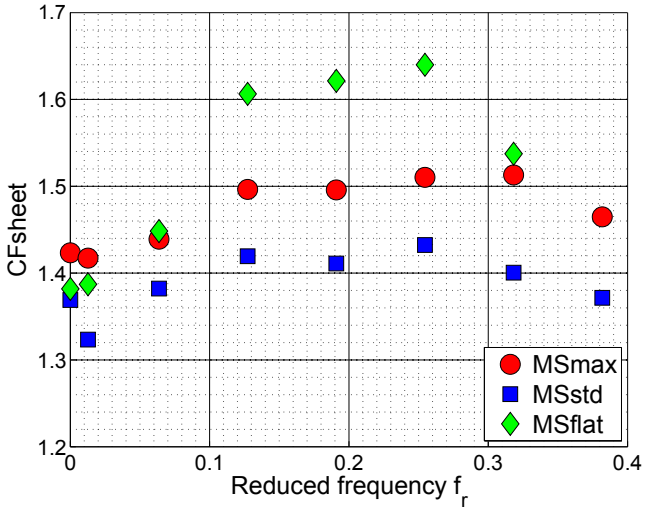

(b) $A = 20\,\mathrm{mm}$

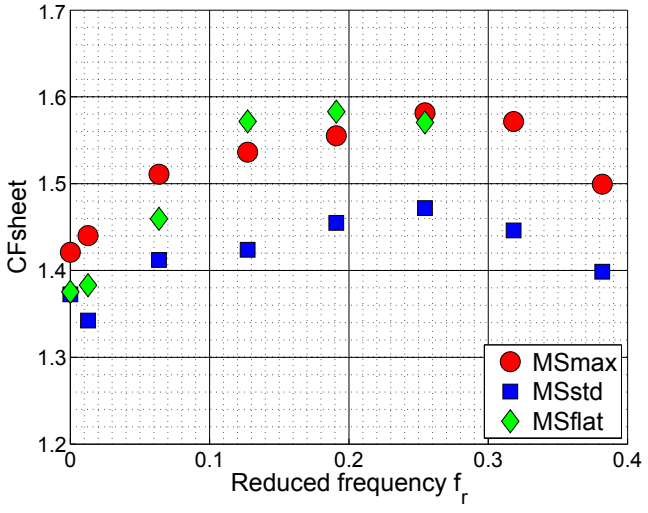

(c) $A = 30\,\mathrm{mm}$

Figure 9: Effect of f_r on CF_{sheet} for the 3 design shape at amplitude (a) $A = 10\,\mathrm{mm}$, (b) $A = 20\,\mathrm{mm}$ and (c) $A = 30\,\mathrm{mm}$.

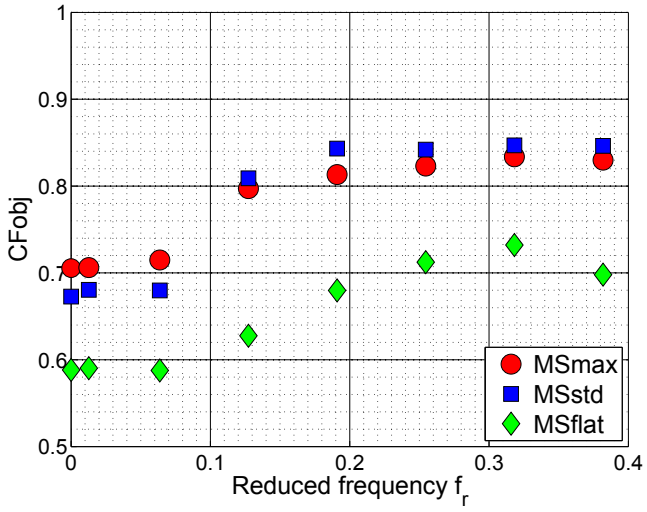

(a) $A = 10\,\mathrm{mm}$

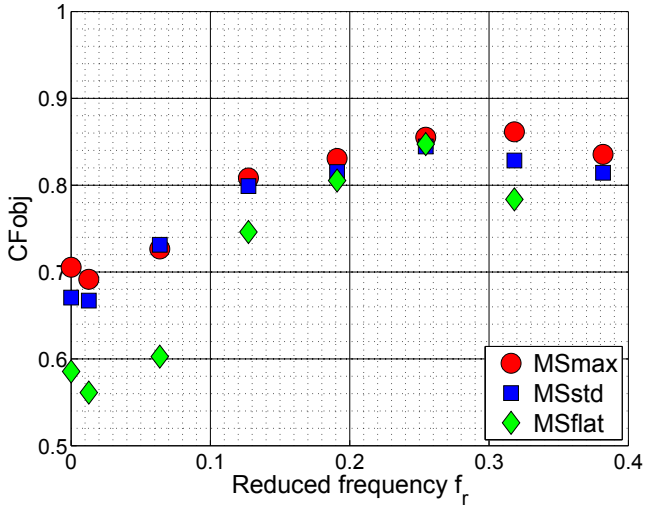

(b) $A = 20\,\mathrm{mm}$

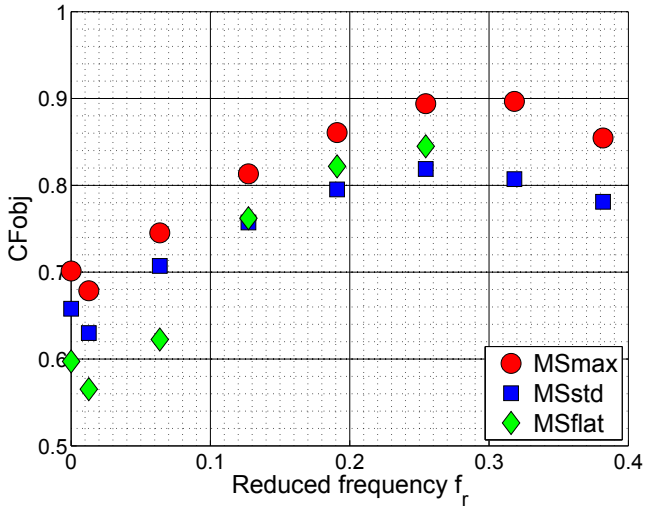

(c) $A = 30\,\mathrm{mm}$

Figure 10: Effect of f_r on CF_{obj} for the 3 design shapes at amplitude (a) $A = 10\,\mathrm{mm}$, (b) $A = 20\,\mathrm{mm}$ and (c) $A = 30\,\mathrm{mm}$.

DISCUSSION

Dynamic contributions to aerodynamic forces can be decomposed into three components. The first one is due to the change in circulation around the profile. At this $AWA = 60°$, the more camber, the more lift in static conditions. The second component is due to the unsteady propulsion caused by the forced oscillation. At a certain range of frequencies studied, flapping might produce vortices structures beneficial to the aerodynamic force produced by the sail. Vortices structures are linked to the sail area, the frequency and the amplitude of oscillation but do not depend on the sail profile. This flapping effect on the flat sail MSflat which suffers from a poor static aerodynamic contribution is then much more significant but on a narrow range of frequencies. The third component is the energy transferred to the system by the oscillation forcing. As mentioned in the section describing the effect of the reduced frequency f_r, mechanical work is given to the system by the forcing in the sheet (Fig. 7). This work is dissipated at most of the frequencies but is beneficial to the thrust at $f_r = 0.255$ (Fig. 8). In the case of a dynamic trimming, the aerodynamic force is composed of the three components with different effects depending on the frequencies and amplitudes of oscillation. It seems that the forcing at $f_r = 0.255$ benefits from all three components, the reason for the local optimum at that frequency.

CONCLUSIONS

An innovative oscillating trimming experiment has been developed in the Twisted Flow Wind Tunnel at the Yacht Research Unit, University of Auckland. The oscillating trimming effect has been studied on different design shapes of IMOCA 60 type mainsails at $AWA = 60°$ with different input parameters: amplitude and reduced frequency. The dynamic oscillations clearly show that quasi-static measurements are not relevant for predicting aerodynamic forces even at quite low reduced frequencies. These results support previous findings that static or quasi-static approaches are not sufficient to capture the complexities of dynamic effects, even for the simplified oscillating trimming simulation.

The sheet load measurement enabled us to calculate the mechanical power transmitted from the trimming device to the entire rig and sail system and could be correlated with the aerodynamic force evolutions of the different sails.

The dynamic effect showed that there was an optimum reduced frequency $f_r = 0.255$ that improved the performance function for the different sails related to a maximum power transmitted to the rig and sails by the sheet. The three different model sails presented the same trends, but the dynamic improvement was more significant for the flat sail: up to an increase of 40% of its CF_{obj} at $f_r = 0.255$ and $A = 30\,\mathrm{mm}$ compared to the steady case.

Oscillations around optimum static trim have also been performed for $AWA = 25°$ and $AWA = 40°$ and will

be compared to this paper's results in a future publication. Flying shape and rig part tracking analysis will also be performed. Further work will be done using those data for comparison and validation of unsteady numerical simulation tools.

ACKNOWLEDGEMENTS

This project has received funding from the European Unions Seventh Program for research, technological development and demonstration under grant agreement N° PIRSES-GA-2012-318924 and from the Royal Society of New Zealand for the UK-France-NZ collaboration project, SAILING FLUIDS (see www.sailingfluids.org). This work was supported by the French Naval Academy, Brest Métropole Océane, Région Bretagne and the Marie Curie European Unions Seventh Framework Programme (FP7/2007-2013) under REA grant agreement n°PCOFUND-GA-2013-609102 (PRESTIGE-Campus France). This work was supported by the "Laboratoire d'Excellence" LabexMER (ANR-10-LABX-19) and co-funded by a grant from the French government under the program "Investissements d'Avenir". The authors are grateful to K-Epsilon and VS-PARS company for their continuous collaboration and to Ronan Floch from Incidence Sails for designing and manufacturing the model-scale sails. The authors would like to thank the SEFER services for providing the electronical actuator and remote control parts, Mr David Le Pelley, wind tunnel manager, and Dr Nick Velychko for their help, guidance, their wise advice and comments.

REFERENCES

CHARVET, T., HAUVILLE, F. and HUBERSON, S., *Numerical simulation of the flow over sails in real sailing conditions*, Journal of Wind Engineering and Industrial Aerodynamics, **63**(1-3), (1996), 111 – 129.

MARCHAJ, C., Sail performance: techniques to maximize sail power, International Marine/Ragged Mountain Press (1996).

GARRETT, R., The symmetry of sailing: the physics of sailing for yachtsmen, Sheridan House, Inc. (1996).

FOSSATI, F. and MUGGIASCA, S., *An experimental investigation of unsteady sail aerodynamics including sail flexibility*, 4th High Performance Yacht Design Conference, Auckland, New Zeeland (2012).

GERHARDT, F., FLAY, R.G.J. and RICHARDS, P.J., *Unsteady aerodynamics of two interacting yacht sails in two-dimensional potential flow*, Journal of Fluid Mechanics, **668**(1), (2011), 551–581.

GERHARDT, F.C., *Unsteady Aerodynamics of Upwind-Sailing and Tacking*, Ph.D. thesis, The University of Auckland (2010).

AUGIER, B., BOT, P., HAUVILLE, F. and DURAND, M., *Experimental validation of unsteady models for fluid structure interaction: Application to yacht sails and rigs*, Journal of Wind Engineering and Industrial Aerodynamics, **101**, (2012), 53–66.

AUGIER, B., BOT, P., HAUVILLE, F. and DURAND, M., *Dynamic Behaviour of a Flexible Yacht Sail Plan*, Ocean Engineering, **66**, (2013), 32–43.

AUGIER, B., HAUVILLE, F., BOT, P., AUBIN, N. and DURAND, M., *Numerical study of a flexible sail plan submitted to pitching: Hysteresis phenomenon and effect of rig adjustments*, Ocean Engineering, **90**, (2014), 119–128.

COLLIE, S. and GERRITSEN, M., *The challenging turbulent flows past downwind yacht sails and practical application of CFD to them*, 2nd High Performance Yacht Design Conference, Auckland, New-Zealand (2006).

DEPARDAY, J., BOT, P., HAUVILLE, F., MOTTA, D., LE PELLEY, D.J. and FLAY, R.G.J., *Dynamic measurements of pressures, sail shape and forces on a full-scale spinnaker*, 23rd HISWA Symposium on Yacht Design and Yacht Construction, Amsterdam (2014).

MASUYAMA, Y., TAHARA, Y., FUKASAWA, T. and MAEDA, N., *Dynamic performance of sailing cruiser by a full scale sea reality*, The 11th Chesapeake Sailing Yacht Symposium, Annapolis, USA (1993).

MASUYAMA, Y. and FUKASAWA, T., *Full scale measurement of sail force and the validation of numerical calculation method*, The 13th Chesapeake Sailing Yacht Symposium, Annapolis, USA (1997).

RICHARDT, T., HARRIES, S. and HOCHKIRCH, K., *Maneuvering simulations for ships and sailing yachts using FRIENDSHIP-Equilibrium as an open modular workbench*, International Euro-Conference on Computer Applications and Information Technology in the Maritime Industries (2005).

KEUNING, J., VERMEULEN, K. and DE RIDDER, E., *A generic mathematical model for the manoeuvring and tacking of a sailing yacht*, The 17th Chesapeake Sailing Yacht Symposium, (143–163), Annapolis, USA (2005).

SCHOOP, H. and BESSERT, N., *Instationary aeroelastic computation of yacht sails*, International Journal for Numerical Methods in Engineering, **52**(8), (2001), 787–803.

RENZSH, H. and GRAF, K., *Fluid Structure Interaction simulation of spinnakers - Getting closer to reality*, 2nd International Conference on Innovation in High Performance Sailing Yachts, Lorient, France (2010).

CHAPIN, V. and HEPPEL, P., *Performance optimization of interacting sails through fluid structure coupling*, 2nd International Conference on Innovation in High Performance Sailing Yachts, Lorient, France (2010).

TRIMARCHI, D., VIDRASCU, M., TAUNTON, D., TURNOCK, S. and CHAPELLE, D., *Wrinkle development analysis in thin sail-like structures using MITC shell finite elements*, Finite Elements in Analysis and Design, **64**, (2013), 48–64.

RANZENBACH, R., ARMITAGE, D. and CARRAU, A., *Mainsail Planform Optimization for IRC 52 Using Fluid Structure Interaction*, 21st Chesapeake Sailing Yacht Symposium, March, (50–58), Annapolis (2013).

DURAND, M., LEROYER, A., LOTHODÉ, C., HAUVILLE, F., VISONNEAU, M., FLOCH, R. and GUILLAUME, L., *FSI investigation on stability of downwind sails with an automatic dynamic trimming*, Ocean Engineering, **90**, (2014), 129–139.

FOSSATI, F., BAYATI, I., ORLANDINI, F., MUGGIASCA, S., VANDONE, A., MAINETTI, G., SALA, R., BERTORELLO, C. and BEGOVIC, E., *A novel full scale laboratory for yacht engineering research*, Ocean Engineering, **104**, (2015), 219–237.

FLAY, R.G.J., *A twisted flow wind tunnel for testing yacht sails*, Journal of Wind Engineering and Industrial Aerodynamics, **63**(1-3), (1996), 171–182.

RENZSCH, H. and GRAF, K., *An experimental validation case for fluid-structure-interaction simulations of downwind sails*, 21st Chesapeake Sailing Yacht Symposium, March, (59–66), Annapolis (2013).

LE PELLEY, D.J., EKBLOM, P. and FLAY, R.G.J., *Wind tunnel testing of downwind sails*, 1st High Performance Yacht Design Conference, (66–75), Auckland (2002).

VIOLA, I.M. and FLAY, R.G.J., *On-water pressure measurements on a modern asymmetric spinnaker*, 21st HISWA Symposium on Yacht Design and Yacht Construction, November, Amsterdam (2010).

FOSSATI, F., Aero-Hydrodynamics and the Performance of Sailing Yachts: The Science Behind Sailing Yachts and Their Design, Adlard Coles Nautical (2010).

FOSSATI, F. and MUGGIASCA, S., *Sails Aerodynamic Behavior in dynamic condition*, The 19th Chesapeake Sailing Yacht Symposium, Annapolis, USA (2009).

FOSSATI, F. and MUGGIASCA, S., *Numerical modelling of sail aerodynamic behavior in dynamic conditions*, 2nd International Conference on Innovation in High Performance Sailing Yachts, Lorient, France (2010).

WRIGHT, A.M., CLAUGHTON, A.R., PATON, J. and LEWIS, R., *Off-wind sail performance prediction and optimisation*, The Second International Conference on Innovation in High Performance Sailing Yachts, Lorient, France (2010).

LASHER, W. and RICHARDS, P., *Validation of Reynolds-averaged NavierStokes simulations for international Americas Cup class spinnaker force coefficients in an atmospheric boundary layer.*, Journal of Ship Reseasrch, **51 (1)**, (2007), 2238.

GRAF, K. and MÜLLER, O., *Photogrammetric Investigation of the Flying Shape of Spinnakers in a Twisted Flow Wind Tunnel*, 19th Chesapeake Sailing Yacht Symposium, March, Annapolis (2009).

VIOLA, I.M. and FLAY, R.G.J., *Sail pressures from full-scale, wind-tunnel and numerical investigations*, Ocean Engineering, **38**(16), (2011), 1733–1743.

VIOLA, I., BOT, P. and RIOTTE, M., *Upwind sail aerodynamics: A RANS numerical investigation validated with wind tunnel pressure measurements*, International Journal of Heat and Fluid Flow, **39**, (2013), 90–101.

FOSSATI, F. and MUGGIASCA, S., *Experimental investigation of sail aerodynamic behavior in dynamic conditions*, Journal of Sailboat Technology, **2**, (2011), 1–41.

LE PELLEY, D. and MODRAL, O., *VSPARS: A combined sail and rig recognition system using imaging techniques*, 3rd High Performance Yacht Design Conference, **14**, (2008), 57–66.

SACHER, M., HAUVILLE, F., BOT, P. and DURAND, M., *Sail trimming FSI simulation - comparison of viscous and inviscid flow models to optimise upwind sails trim*, 5th High Performance Yacht Design Conference, (217–228), Auckland, New-Zealand (2015).

SACHER, M., HAUVILLE, F., DUVIGNEAU, R., LE MAITRE, O., AUBIN, N. and DURAND, M., *Experimental and numerical trimming optimizations for a mainsail in upwind conditions*, The 22nd Chesapeake Sailing Yacht symposium, Annapolis, Maryland (2016).

SCHAFER, R., *What Is a Savitzky-Golay Filter?*, IEEE Signal Processing Magazine, **28**(4), (2011), 111–117.